RSC Advances

PAPER

View Article Online
View Journal | View Issue

Cite this: *RSC Adv.*, 2024, **14**, 38171

Release characteristics of biochar-derived dissolved organic matter and its impact on Cr(VI) adsorption and reduction†

Hui Liu,‡ Ying Wang,‡ Shixu Wang, Jing Wu and Yulai Wang *

Biochar has received widespread attention as a promising amendment for heavy metal stabilization due to its abundant porosity and surface functional groups. However, the role of biochar-derived dissolved organic matter (BDOM) is usually overlooked. In this study, we systematically investigated the leaching dynamics of BDOM from garden wastes through hydrothermal carbonization (HC), pyrolysis (PC) and hydro/pyrolysis (HPC) and explored their impacts on Cr(VI) environmental behavior in an extremely acidic environment. Results showed that BDOM leaching dynamics followed the first order model, and HC leached more BDOM than PC and HPC, especially for Ar-P, SMP and Ha-L fractions. Although carbonized using various methods, the biochars displayed a similar adsorption capacity for Cr(VI) at an environmental-related concentration of 2 mg L^{-1}. The presence of BDOM accelerated the Cr(VI) adsorption rate on biochars due to their pre-complexing. Simultaneously, HC-BDOM acted as an electron donor and participate in Cr(VI) reduction directly, resulting in the synchronous reduction of Cr(VI) during its adsorption process. However, PC- and HPC-BDOM preferentially acted as electron acceptors, thus competing with Cr(VI) for Fe(II) oxidation and decreased the Cr(VI) reduction rate. This study suggested that biochar from garden wastes has a great remediation potential for Cr-contaminated land and that BDOM (especially HC-BDOM) plays a significant role in increasing soil organic matter, stabilizing heavy metals and detoxifying toxic substances by oxidation-reduction.

Received 26th August 2024
Accepted 18th November 2024

DOI: 10.1039/d4ra06172a

rsc.li/rsc-advances

1. Introduction

Chromium (Cr) is a common aquatic and soil contaminant commonly found in industrial wastewater from sectors such as steel production, metallurgy, tanning, and electroplating, as well as in brownfields, including abandoned mining and industrial sites and land used for manufacture and storage. In China, the distribution of Cr concentrations were 14.88–98.08 mg kg^{-1} in mining-brownfield and 600–5000 mg L^{-1} in various industrial wastewater.[1,2] Cr is highly reactive with oxidation states ranging from −2 to +6. In the natural environment, Cr(III) and Cr(VI) are the predominant forms influenced by pH and redox conditions.[3,4] Compared to Cr(III), Cr(VI) is hypertoxic and carcinogenic due to its greater solubility and ability to rapidly penetrate through cell membranes.[5,6] Based on the above, reducing Cr(VI) to Cr(III) is an effective way to reduce its eco-environmental risks. However, we should be aware that Cr(III) would be redissolved under extremely acidic conditions and might even be reoxidized to Cr(VI) under oxidizing conditions.[7,8] Hence, the real environmental conditions in the treatment of Cr-containing wastewater treatment or Cr-contaminated brownfield remediation, such as low pH, environmental-related Cr concentration and its oxidation states, should be thoroughly considered.

Biochar is a renewable and cost-effective carbonaceous material derived from widespread biomass, including agricultural and garden residues, kitchen wastes, sludge and livestock wastes, and has attracted increasing attention in wastewater treatment and contaminated land remediation due to its availability, low cost, environmental friendliness, and sustainability as a stabilizer.[9,10] Intensive research has demonstrated that biochar has a high potential for heavy metal immobilization because of its abundant porosity and surface functional groups.[11] The porous carbon skeletal structure of biochar can provide multi-functions in the treatment and remediation of a Cr-contaminated environment, as follows: (i) biochar usually shows high adsorption affinity for Cr because of abundant porosity and surface groups,[12] which can reduce the adsorbed Cr(VI) to Cr(III) and further bind Cr(III) through physisorption, complexation and ion-exchange mechanisms,[13,14] thus decreasing the mobility and toxicity of Cr.[15,16] (ii) Microbial abundance and diversity increase after biochar application in Cr-contaminated wastewater and lands. This is largely because of the porous structure, which could provide a physical refuge

School of Energy and Environment, Anhui University of Technology, Maanshan City 243002, China. E-mail: yulai_wang@163.com

† Electronic supplementary information (ESI) available. See DOI: https://doi.org/10.1039/d4ra06172a

‡ These authors contributed equally to this work.

for microorganisms, and the released chemical compounds might stimulate soil microbial activity.[17] In addition, (iii) the soil carbon sink was enhanced after applying biochar in Cr-contaminated land, which was due to the increase in soil aggregate stability caused by the biochar-induced negative priming effect.[18,19] However, the detailed adsorption and reduction processes of Cr in a real environment, especially under extremely acidic and anaerobic conditions, must be studied in-depth.

Biochar application releases inorganic elements and biochar-derived dissolved organic matter (BDOM), which could improve the fertility of contaminated brownfields.[17,20] Biochar contains multiple metallic ions (Ca, Mg, K, *etc.*) and non-metallic ions (*e.g.*, P) that can leach during long-term applications.[21,22] However, previous studies indicated that biochar could be aged by natural oxidants, microbial agents, ultraviolet radiation and mechanical fragmentation, which resulted in the release of BDOM.[23,24] The BDOM of biochar is generally defined as the soluble organic components that remain in biochar, and it mainly includes *n*-alkanoic, benzoic, hydroxyl, acetoxy, amines, and phenols, as well as N-, O-, and S-containing heterocyclic compounds.[25] Recent reports revealed that BDOM played vital roles in the migration and oxidation-state conversion of heavy metals (*i.e.*, Cr, As, and Pb), the high aromaticity and relatively large molecular weight of BDOM contributed to its complexation ability with heavy metals, and rich-conjugated groups in BDOM triggered its oxidation-reduction reactions,[26,27] For example, BDOM could serve as electron donors for Cr(VI) reduction and also as electron acceptors for As(III) oxidation.[28] However, the ecological functions of BDOM have often been overlooked, and the BDOM leaching dynamics in a real environment and their impact on the environmental behaviors of heavy metals are rarely reported.

Therefore, we proposed that carbonization pathways would influence the "quantity" and "quality" of BDOM and consequently lead to differences in the organic matter supply and the fates of heavy metals after biochar application. To systematically evaluate the release of BDOM and its impact on the adsorption–reduction behavior of Cr(VI) under extremely acidic and anaerobic conditions. In this study, hydrochar (HC), pyrochar (PC) and hydro–pyrochar (HPC) were carbonized from garden wastes, and the roles of BDOM on the immobilization and reduction of Cr(VI) were evaluated. The designed experimental processes are shown in Fig. 1. The main objectives were to (i) investigate the leaching capabilities of BDOM and quantitatively evaluate their kinetics; (ii) explore the effects of leached BDOM on the adsorption of Cr(VI) under low pH conditions; and (iii) evaluate the influence of BDOM on Cr(VI) reduction. These results would improve the understanding of the contributions of BDOM in Cr-contaminated brownfield reclamation.

2. Materials and methods

2.1 Chemicals and materials

A stock solution of Cr(VI) was prepared by dissolving an appropriate amount of $K_2Cr_2O_7$ in deionized water. 1,5-Diphenylcarbohydrazide and 1,10-phenanthroline were purchased from Sinopharm Chemical Reagent Co. Ltd (Shanghai, China). All the chemicals used in this study were of analytical grade and were used without further purification.

2.2. Biochars and their BDOM preparation

Garden wastes, mainly constituted of sticks and litter from *Firmiana simplex*, were collected and dried at 60 °C for 12 h, and

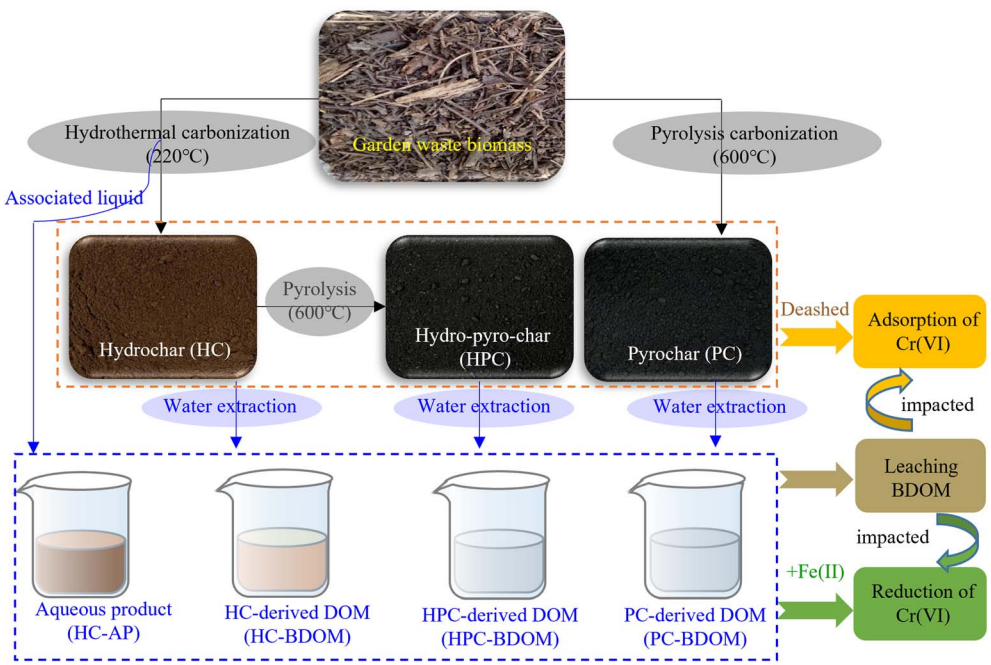

Fig. 1 The designed experimental processes in the present study.

then ground into powder. The biomass powder was used to produce three types of biochar, including HC, PC and HPC, according to the literature.[29,30] For HC, 8 g biomass was hydrothermal with 50 mL deionized water carbonized at 220 °C for 4 h. The HC was obtained by filtering with 0.45 μm polyvinylidene fluoride filters (PVDF, Merck Millipore), followed by drying at 80 °C for 12 h. Meanwhile, the hydrothermal carbonization aqueous product (HC-AP) was collected and saved in a brown bottle at 4 °C to reduce Cr(VI). The PC was obtained by pyrolysis of 20 g biomass at 600 °C for 2 h under N_2 conditions with a flow rate of 100 mL min^{-1} and a heating rate of 5 °C min^{-1}. The HPC was pyrolyzed from the HC using the same method as the PC.

BDOM was extracted from HC, PC and HPC using deionized water and conducted in a sealed flask with a solid-to-liquid ratio of 1 : 20.[31] In brief, 5 g of biochar was suspended in 100 mL of deionized water, stirred at 25 °C for 24 h and then filtered through 0.45 μm PVDF. These filtrates from HC, PC and HPC were denoted as HC-BDOM, PC-BDOM and HPC-BDOM, respectively, and saved in brown bottles at 4 °C, and used to reduce Cr(VI).

The HC, PC and HPC were deashed using a mixed acid solution of 3% HCl and 10% HF.[32] Briefly, HC, PC and HPC were dispersed in the mixed acid with a solid-to-liquid ratio of 1 : 5. The suspension was shocked at 40 °C for 24 h and then centrifuged to remove the supernatant. After six mixed acid treatments, the sample was washed to neutral with deionized water, followed by drying at 80 °C. The deashed HC, PC and HPC were named D-HC, D-PC and D-HPC, respectively.

2.3 Batch experiments

2.3.1 Leaching of BDOM and their dynamics. The BDOM leaching tests from biochar were carried out in shake flasks with a solid-to-liquid ratio of 1 : 80, and the leachate was collected at pre-set intervals, filtered by 0.45 μm PVDF, and analyzed for DOC content, UV-Vis and fluorescent spectra. All experiments were conducted in triplicate. The BDOM leaching dynamics were analyzed according to the first-order kinetic model, as described in eqn (1):[33]

$$y = y_0 + ae^{-kt}, \quad (1)$$

where y is the leaching amount measured over time t, y_0 is the maximum leaching capacity, a is the constant that represents the leaching intensity and k is the first-order rate constant.

2.3.2 Adsorption of Cr(VI) on biochars and their dynamics. To evaluate Cr(VI) fixation on biochars in a real acidic environment, the adsorption dynamics of Cr(VI) were determined with 0.5 g L^{-1} biochar and 2 mg L^{-1} Cr(VI). The initial solution pH was adjusted to 2.0 using HNO_3. The concentration of Cr(VI) was measured with a UV-Vis spectrophotometer using the 1,5-diphenylcarbazide method after filtration through 0.45 μm PVDF. The adsorption rates were analyzed according to the pseudo-first-order and pseudo-second-order kinetic models, as described in eqn (2) and (3),[34] respectively:

$$\ln(q_e - q_t) = \ln q_e - k_1 t, \quad (2)$$

$$\frac{t}{q_t} = \frac{1}{k_2 {q_e}^2} + \frac{t}{q_e}, \quad (3)$$

where q_e is the equilibrium adsorption amount (mg g^{-1}), q_t is the adsorption amount (mg g^{-1}) at time t (h), and k_1 and k_2 are the pseudo-first-order rate constant and pseudo-second-order rate constant, respectively.

2.3.3 Reduction of Cr(VI) by BDOM and BDOM-Fe(II) systems. The Cr(VI) reduction experiments were performed under dark conditions at pH 2.0 with Cr(VI), Fe(II) and BDOM initial concentrations of 2 mg L^{-1}, 4 mg L^{-1}, and 0–10 mg L^{-1}, respectively. The concentration of Fe(II) was measured with a UV-Vis spectrophotometer using the phenanthroline method, and the total Cr and total Fe were detected using an atomic absorption spectrophotometer. All experiments were performed in triplicate, and the Cr(VI) reduction dynamics were fitted using a single exponential model (eqn (4)):

$$C_t/C_0 = F_1 + F_2 e^{-kt}, \quad (4)$$

where C_t is the Cr(VI) concentration at time t (h), C_0 is the Cr(VI) initial concentration, k is the rate constant (h^{-1}), and F_1 and F_2 are the relative amounts (%) of the unreduced Cr(VI) and reduced Cr(VI), respectively.

2.4 Biochars and BDOM characterization

The specific surface area (S_{BET}) and pore size distributions of the biochar were determined on an ASAP 2460 (Micromeritics Instrument Co., USA) at −196 °C (77 K). Prior to the nitrogen adsorption measurements, the samples were outgassed at 300 °C for 3 h under vacuum. The FT-IR spectra of biochar were obtained using a Nicolet6700 FT-IR spectrometer with a 4 cm^{-1} resolution.

The BDOM extracted from biochar was determined by applying a Shimadzu TOC-V_{CPH} analyzer. UV-Vis spectra of BDOM were measured by applying a TU-1901 spectrophotometer with a wavelength range of 200–700 nm and 1 nm increment. The chromophoric DOM quantities were represented using a_{280}, and special UV optical indices (including $SUVA_{254}$, E_2/E_3 and $S_{275-295}$) were calculated according to the literature.[35–37] In addition, EEMs of BDOM (F_{BDOM}) were measured by applying a Hitachi F-4500 spectrofluorometer with an excitation/emission wavelength range of 220–400 nm/250–550 nm. The obtained EEM was analyzed using fluorescence regional integration (FRI),[38,39] which divided the EEM into four components: aromatic protein-like (Ar-P), fulvic acid-like (Fa-L), soluble microbial by-product (SMP) and humic acid-like (Ha-L).

2.5 Data statistical analysis

In this study, all experiments (including BDOM leaching, Cr(VI) adsorption and reduction) were conducted independently in triplicate, and the average values and their standard deviations were calculated. The dynamics of BDOM leaching, adsorption and reduction of Cr(VI) were fitted using a nonlinear regression model on Origin 8.0 software. Simultaneously, the differences in the kinetic parameters among the three treatments were determined using Duncan's multiple range test with P-values of

0.05 and 0.01 on the Statistical Program for Social Sciences (SPSS, Version 13.0).

3. Results and discussion

3.1 Characterization of biochars and their BDOM

The typical IV N_2 adsorption–desorption isotherms and pore size distributions shown in Fig. S1† indicated that PC and HPC consisted of microporosity and mesoporosity, while HC was preponderant for mesoporous structure.[40] This was because a high temperature during the pyrolysis process was helpful for pore development.[41] The S_{BET} values and pore structure parameters listed in Table 1 showed much higher S_{BET} and total pore volume of HPC compared to PC and HC, which profited from the continuous hydrothermal-pyrolysis carbonization that enhanced the decomposition and volatilization of organic matter. The similar shape curve of FT-IR shown in Fig. S2† indicated that HC, PC and HPC consisted of the same types of functional groups. Three main absorption characteristic peaks were identified at 3200–3700 cm^{-1}, 2850–2930 cm^{-1} and 1000–1800 cm^{-1}, representing hydrogen bonding, aliphatic structures and oxygen-containing functional groups, respectively.[42,43] The stronger intensity of characteristic peaks observed on HC suggested that HC consisted of more functional groups than PC and HPC, which was because of its weak carbonation degree.[42,44]

The UV/Vis-spectra of HC-AP and extracted BDOM from HC, PC and HPC are shown in Fig. S3.† A shoulder peak was observed on HC-AP and HC-DOM in a wavelength range of 250–300 nm, which was generally related to the π–π electron transition of C=C and C=O double bond groups.[37] This demonstrated that HC-AP and HC-DOM contained many aromatic or unsaturated reductive compounds, such as phenols, aniline derivatives, polyenes and polycyclic aromatic substances.[37,45,46] The UV-Vis spectral indicators of DOM were calculated, as listed in Table S1.† The higher $S_{275-295}$ and lower $SUVA_{280}$ values of PC-DOM and HPC-DOM represented lower aromaticity and molecular weight than those of HC-AP and HC-DOM, which could be ascribed to the decomposition of aromatic components with large molecules into small molecules during the pyrolysis process.[31]

3.2 Leached BDOM quantity and its fluorescent components

The variations of bulk BDOM (including BDOC contents, a_{280} and F_{BDOM}) leached from HC, PC and HPC were analyzed, as depicted in Fig. 2. The bulk BDOM quantities were leached rapidly within the initial 20 min, which contributed to 42–80% of their total leached amounts. After initial rapid leaching, these BDOM quantities increased gradually until they reached an equilibrium state within 24 h. These were similar to the trends of extractable DOM leached from sediment into the natural water body.[33]

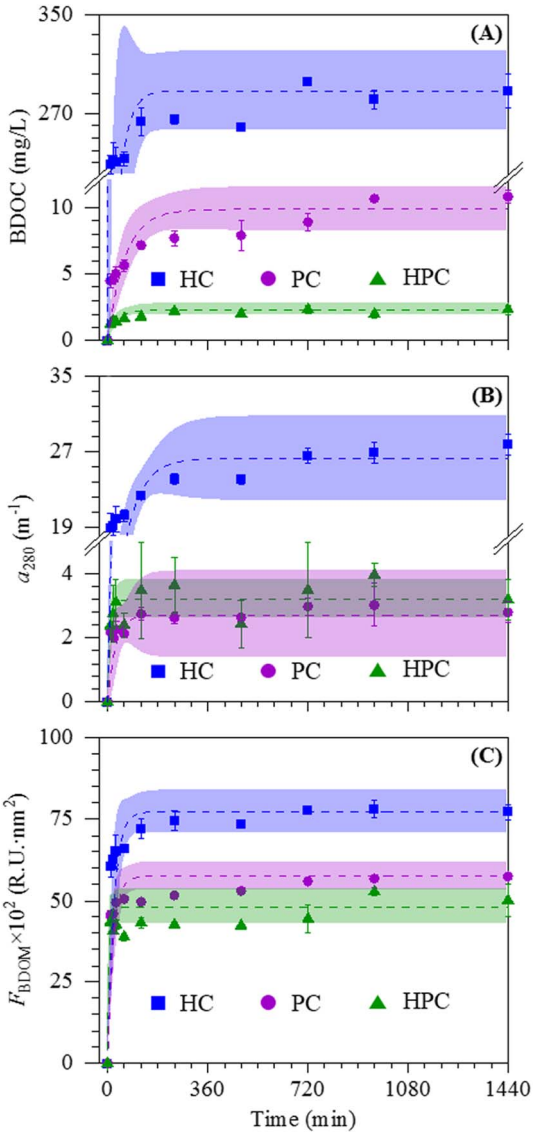

Fig. 2 The leaching trends of BDOC content with solid-to liquid ratio of 1 : 80 for DOC contents (A), chromophoric BDOM (B) and fluorescent BDOM (C) from HC, PC and HPC.

Table 1 BET surface area and pore structure of biochars

Biochars	S_{BET} (m^2 g^{-1})	Total pore volume[a] (cm^3 g^{-1})
HC	7.25	0.0162
PC	27.93	0.0213
HPC	286.51	0.1639

[a] Determined at $P/P_0 = 0.97$.

The leaching dynamics of BDOM from HC, PC and HPC were also analyzed. Fig. 2A–C demonstrates that the BDOM leaching processes were well fitted with the first order kinetics model ($P < 0.001$) with R^2 ranging from 0.87 to 0.99. The theoretically calculated leaching BDOC amounts by the first order model were 288.49, 9.84 and 2.29 mg L^{-1} for HC, PC and HPC, respectively (Table S2†). Similarly, the theoretically calculated chromophoric BDOM (a_{280}) and F_{BDOM} leaching quantities also followed the order of q_e(HC) > q_e(PC) ≥ q_e(HPC) (Table S2†). These results demonstrated that biochar from hydrothermal carbonization leached more BDOM into the environment than

that from pyrolysis because the decomposed organic matter mainly remained in the pore structure of HC during the hydrothermal carbonization process.[31,47] Simultaneously, there were also differences in BDOM leaching rates between hydrochars and pyrochars. The BDOM leaching rates (k values, Table S2†) of the HPC were higher than those of the HC and PC. As described above, HPC possessed more abundant pore structures than HC and PC, and the most organic matter inside HPC pore structures was decomposed and released during the continuous hydrothermal-pyrolysis carbonization process, which was in favor of BDOM release.[48]

To further probe the variations of fluorescent components from BDOM after application, we divided BDOM into the four fluorescent components (Ar-P, Fa-L, SMP and Ha-L) by EEMs combined with the FRI technique (Fig. S4A–C†), and calculated their relative contributions of Ha-L, Fa-L, SMP and Ar-P to bulk BDOM with 52.13–54.47%, 16.16–19.58%, 14.08–17.03% and 12.14–14.4%, respectively (Fig. S4D–F and Table S3†). Similarly, the leaching trends of Ar-P, Fa-L, SMP and Ha-L components derived from HC, PC and HPC also followed the first-order dynamics (Fig. 3A–D). Their kinetic parameters are shown in Table S2.† We also found that the leached Ar-P, SMP and Ha-L quantities from HC were always larger than those from PC and HPC. Simultaneously, the theoretically calculated leaching rates of Ar-P and Fa-L from PC and HPC were faster than those from HC, while there were more complicated changes in the leaching rates for the SMP and Ha-L components from the different biochars. The above results demonstrated that hydrochars leach more Ar-P, SMP and Ha-L substances compared to pyrochars after application. Despite the diversity in leaching rates of Ar-P, Fa-L, SMP and Ha-L among HC, PC and HPC, their relative contributions kept stable levels for HC, PC and HPC, respectively.

The leaching characteristics of BDOM from HC, PC and HPC suggested that biochar possessed a high potential for soil fertility improvement, and the amount and structure of released BDOM were significantly influenced by their carbonization methods. Additionally, intensive studies have demonstrated that the different biochar resources lead to various structural compositions of BDOM.[49] Bandara *et al.*[12] indicated that the biochar could be a source of organic contaminants (such as volatile organic compounds, polycyclic aromatic hydrocarbons, and dioxins) and heavy metals (such as Cr, Mn, Cu, and Zn). These contaminants were either present in the biomass or produced during the carbonization process and could be released along with BDOM during long-term application. Thus, we should also pay attention to the influence of biochar resources, especially those containing toxic and harmful substances, such as sewage sludge and biomass from heavy metal-contaminated soil, which may pose higher ecological risks.[50] Although the biomass used in this study was uninvolved in the abovementioned materials, the potential toxicity still must be further evaluated before large-scale applications.

3.3 Adsorption kinetics of Cr(VI) on biochars and their influences

To elucidate the influence of BDOM on heavy metal immobilization, the adsorption dynamics of environmental Cr(VI) content (2 mg L^{-1}) on biochars (Fig. 4A and B) and deashed biochars (Fig. 4C and D) (including D-HC, D-PC and D-HPC)

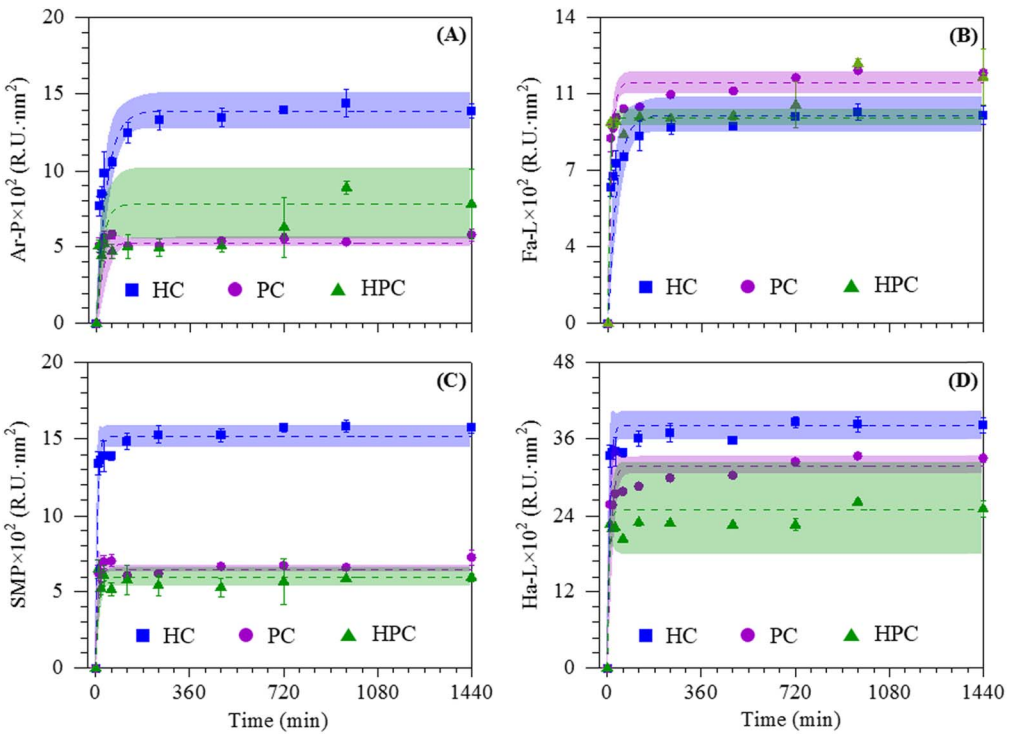

Fig. 3 The leaching trends of Ar-P (A), Fa-L (B), SMP (C) and Ha-L (D) derived from HC, PC and HPC with solid-to liquid ratio of 1 : 80.

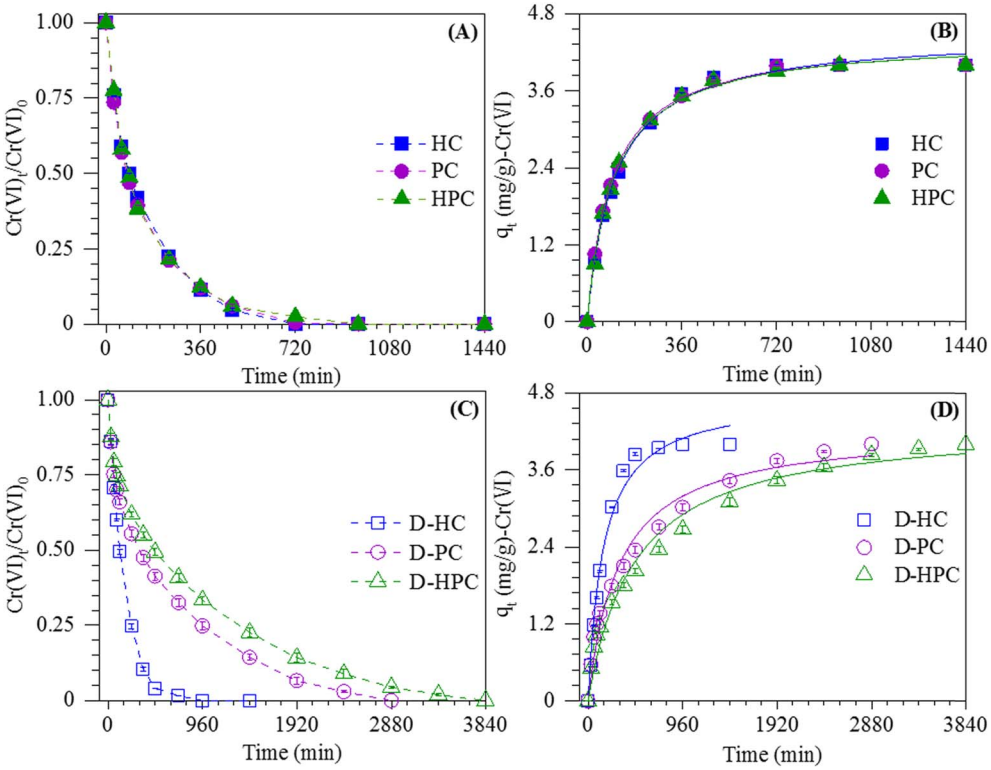

Fig. 4 The adsorption kinetics of Cr(VI) on biochars (A, B) and deashed biochars (C, D). Experimental conditions: pH 2; biochar dosage: 0.5 g L; Cr(VI) initial concentration: 2 mg L^{-1}.

were conducted in this study. We observed that all biochars could retain 98% ± 2% of Cr(VI), regardless of whether they were deashed or not. However, the Cr(VI) adsorption on HC, PC and HPC achieved an equilibrium state within 12 h, while D-HC, D-PC and D-HPC achieved an equilibrium state within 16 h, 48 h and 64 h, respectively. In addition, the pseudo-first order and pseudo-second order models were used to fit the adsorption kinetics of Cr(VI) (Table S4†). The fitting results showed that the Cr(VI) adsorption progress could be better described by the pseudo-second order model (R^2 > 0.98, P < 0.001), and the adsorption rates of Cr(VI) on deashed biochars were slower than those without deashing treatment.

As shown in Subsection 3.1, HC, PC and HPC exhibited various surface and pore structures, which certainly influence Cr(VI) adsorption performance over biochars. However, similar adsorption capacities were observed in this study. FT-IR analysis showed that the surface of biochar was rich in O-containing functional groups, which could bind Cr(VI) through surface complexation, hydrogen bonding and electrostatic interaction.[51,52] Although HC had lower S_{BET} and total pore volumes compared to PC and HPC, the similar Cr(VI) adsorption capacity observed on HC could be attributed to its abundant surface functional groups. Additionally, the slowed adsorption rate of Cr(VI) on deashed biochars could be attributed to the leaching of minerals and BDOM. According to the literature, the minerals in biochar could enhance Cr adsorption on biochar through ion exchange.[41] Moreover, He *et al.*[13] suggested that BDOM in biochars introduces additional functional groups, thereby enhancing heavy metal adsorption and altering their adsorption behavior. These results suggested that the biochars were of great potential for Cr(VI) fixation even when BDOM and minerals were leached during long-term applications under extremely acidic conditions, and BDOM in biochars played important roles in accelerating Cr(VI) adsorption rates.

3.4 Influences of BDOM on Cr(VI) reduction

It was noteworthy that Cr(III) was also detected in the biochar adsorption systems with a range of 0.54–1.29 mg L^{-1} (Fig. S5†), which indicated that a portion of Cr(VI) was reduced into Cr(III) owing to the reductive substances in adsorption systems. To clarify the influences of BDOM on the reduction capacity of Cr(VI) after biochar application, we conducted the simulated Cr(VI) reduction experiments using only BDOM and BDOM-Fe(II) systems.

Cr(VI) reduction efficiencies by direct BDOM showed that HC-derived BDOM (including HC-AP and HC-BDOM) of 1–10 mg C L^{-1} could reduce 4–10% of Cr(VI), and the reduction efficiency improved with increasing BDOM content (Fig. 5A and B). However, no obvious reduction of Cr(VI) by direct PC- and HPC-BDOM was observed (Fig. 5C and D). The UV/Vis spectra analysis indicated that HC-AP and HC-BDOM contained more unsaturated reductive compounds, which could explain their higher reducibility for Cr(VI) than pyrochar-derived BDOM.

Considering that ferrous oxides are widely distributed in the environment, the reduction efficiency of BDOM to Cr(VI) in the presence of Fe(II) was evaluated in this study (Fig. 6). We observed that the reductive trends of Cr(VI) by BDOM-Fe(II) fitted

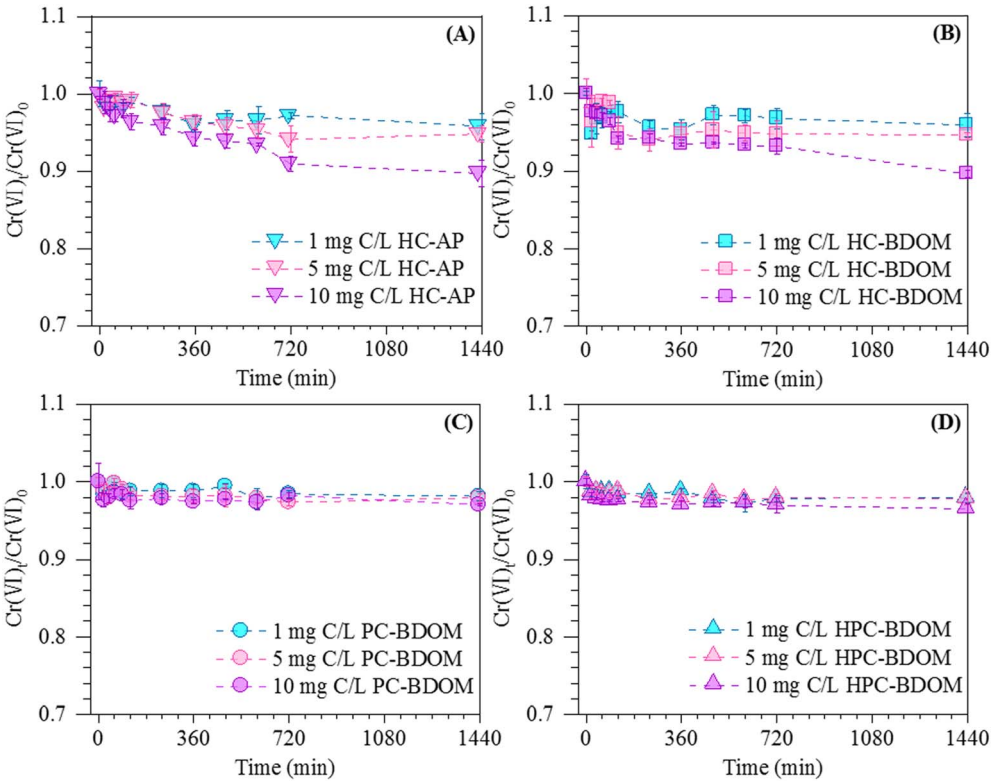

Fig. 5 The reduction of Cr(VI) by direct HC-AP (A), HC-BDOM (B), PC-BDOM (C) and HPC-BDOM (D). Experimental conditions: pH 2; Cr(VI) initial concentration: 2 mg L^{-1}.

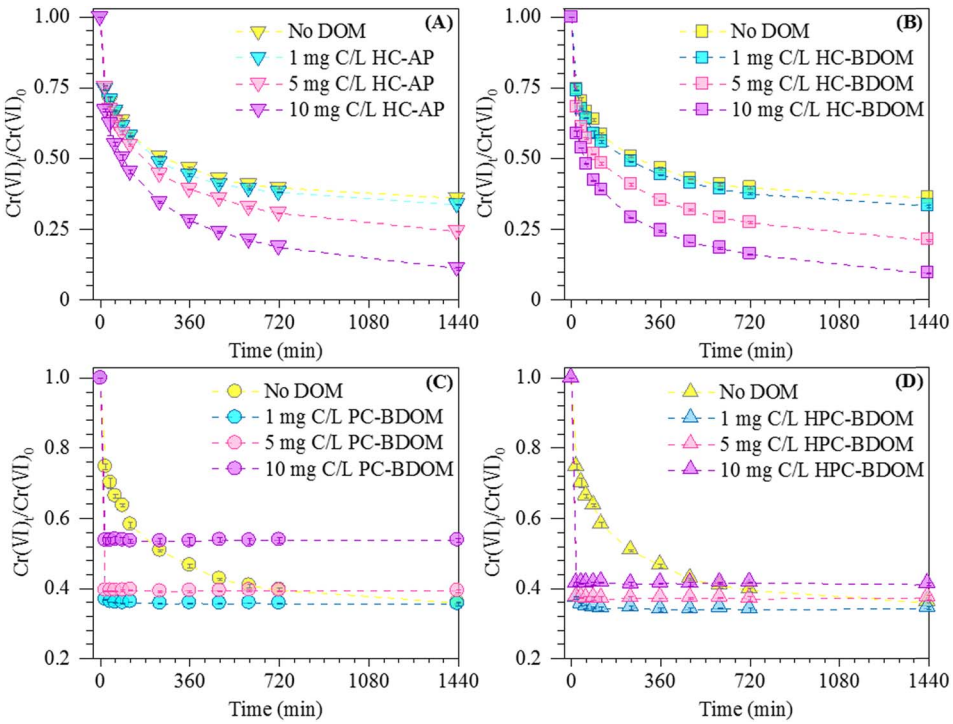

Fig. 6 The reduction of Cr(VI) by Fe(II) under the mediation of HC-AP (A), HC-BDOM (B), PC-BDOM (C) and HPC-BDOM (D). Experimental conditions: pH 2; Cr(VI) initial concentration: 2 mg L; Fe(II) initial concentration: 4 mg L^{-1}.

well to the single exponential model ($R^2 > 0.99$ and $P < 0.01$, Table S5†). The fitting results showed that Cr(VI) reduction amounts and rates increased in the presence of hydrochar-derived BDOM (Fig. 6A and B), and the Cr(VI) reduction efficiencies increased by 16.80% and 17.13% at HC-AP and HC-BDOM contents of 10 mg C L^{-1}, respectively (Table S5†). However, PC-BDOM and HPC-BDOM exhibited a slight decrease in the reductive amounts of Cr(VI), which also significantly accelerated Cr(VI) reduction rates (Fig. 6C and D). These findings indicate that BDOM served as an electron shuttle in the Cr(VI) reduction and altered the reduction efficiency after biochar's application.

To further explore the impacts of hydro- and pyro-char-derived BDOM on Cr(VI) reduction processes, we monitored the variation trends of Fe(II) contents during the reduction reactions (Fig. S6†) and calculated their molar ratios of the oxidized Fe(II) to the reduced Cr(VI) (Δ[Fe(II)]/Δ[Cr(VI)]) (Table 2). Without BDOM, the Δ[Fe(II)]/Δ[Cr(VI)] ratio was calculated to be 2.0, which is lower than the theoretical molar stoichiometry of 3.0; this may be due to the complexation of Cr(VI) and Fe hydroxides produced during the reaction of Cr(VI) and Fe(II).[7] However, the results showed that the Δ[Fe(II)]/Δ[Cr(VI)] ratios in the HC-AP and HC-BDOM systems were lower than those in the control treatment, and they decreased as the HC-AP and HC-BDOM contents increased. These findings demonstrated that hydrochar-derived BDOM could serve as an electron donor for Cr(VI) reduction, which contributed to the increased Cr(VI) reduction amounts with increasing hydrochar-derived BDOM.[53]

However, the Δ[Fe(II)]/Δ[Cr(VI)] ratios in the PC-AP and HPC-BDOM systems were larger than those in the control treatment and increased from 2.47 ± 0.15 to 3.44 ± 0.25 and from 2.66 ± 0.11 to 3.03 ± 0.15 with the PC-BDOM and HPC-BDOM increasing from 1 to 10 mg C L^{-1}. Additionally, almost all Fe(II) was oxidized to Fe(III) within 20 min in the presence of PC- and HPC-BDOM (Fig. S6C and D†). This indicated that pyrochar-derived BDOM (including PC- and HPC-BDOM) served as an electron acceptor and competed with Cr(VI) for Fe(II) oxidation, which could explain the decrease in Cr(VI) reduction amounts as PC- and HPC-BDOM contents increased.

3.5 Environmental implications

Biochar has drawn much attention due to its promising performance in improving soil fertility, activating microbial activity and immobilizing contaminates.[54–56] The application of biochar in heavy metal-polluted land and wastewater remediation could achieve the concept of "treating the wastes with wastes". To explore the potential of garden wastes-derived biochar for the remediation of Cr-contaminated land, the present study synthesized *Firmiana simplex*-derived biochars by hydrothermal carbonization, pyrolysis, and hydrothermal–pyrolysis carbonization. Our results showed that hydrochars would release more BDOM, especially for Ar-P, SMP and Ha-L substances, into the environment compared to pyrochars (Fig. 2, 3 and Table S1†). These findings indicated that the released BDOM met the need for increasing soil organic matter after biochar's application,[25,57] and improved its fertility (*e.g.*, K, Ca, Mg, and Si) for infertile soils, such as abandoned mining, saline, and industrial waste lands.[54] However, it was worth noting that the impacts of biochar amendment on soil organic carbon pool and its mineralization were divergent due to biochar feedstock types, carbonization conditions and soil environment.[58–60] Hence, we should evaluate the impact of BDOM and its derived roles (such as organo–mineral interactions and microbial carbon pump) on soil carbon sequestration and mitigating climate change through long-term field experiments.

Furthermore, to explore the effects of BDOM on the environmental behavior of Cr(VI), this study investigated the influence of BDOM on Cr(VI) adsorption and reduction and analyzed the possible mechanism. The results showed that BDOM would accelerate the Cr(VI) adsorption onto biochars (Table S3†); the possible explanation was the pre-complexation, and the formation of BDOM-Cr complexes preferred to adsorb onto the biochar skeleton due to the varied surface electronegativity.[61,62] In addition, BDOM contains a series of functional groups, such as –C–O and –C=O, which facilitates the reduction of heavy metals (*e.g.*, As(V) and Cr(VI)).[63,64] Our results proposed that hydrochar-derived BDOM exhibited higher aromaticity and molecular weight compared to pyrochar-derived BDOM, which served as an electron donor for Cr(VI) reduction, and they increased the Cr(VI) reduction amount and accelerated its reduction rate (Fig. 6A and B). Moreover, pyrochar-derived BDOM preferred to act as an electron acceptor and competed with Cr(VI) for Fe(II), which could lead to the loss of Fe(II) and decreased Cr(VI) reduction efficiency. Consequently, we should not overlook the contributions of BDOM to the immobility and reduction of Cr(VI) after biochar amendment in practice, and hydrochar may exhibit better remediation performance in Cr(VI)-contaminated wastewater and lands.

Table 2 The molar ratios of the oxidized Fe(II) to the reduced Cr(VI) in Cr(VI) reduction reactions by Fe(II) under the mediation of different BDOM systems

	Δ[Fe(II)]/Δ[Cr(VI)] in different reaction systems			
BDOM concentration	HC-AP	HC-BDOM	PC-BDOM	HPC-BDOM
0 mg C L^{-1}	2.00 ± 0.51			
1 mg C L^{-1}	1.93 ± 0.51	1.80 ± 0.57	2.47 ± 0.15	2.66 ± 0.11
5 mg C L^{-1}	1.47 ± 0.64	1.71 ± 0.32	2.69 ± 0.17	2.81 ± 0.13
10 mg C L^{-1}	1.12 ± 0.47	1.28 ± 0.30	3.44 ± 0.25	3.03 ± 0.15

4. Conclusions

This study systematically investigated the leaching dynamics of BDOM from garden waste-derived biochars obtained by hydrothermal carbonization, pyrolysis and hydro/pyrolysis and explored their effects on Cr adsorption and reduction. The results showed that the BDOM leaching dynamics followed the first-order model, and HC would leach more BDOM (288.49 mg C L^{-1}) than PC and HPC, which were 9.84 mg C L^{-1} and 2.29 mg C L^{-1}, respectively. The BDOM exhibited the characteristics of high aromaticity and large molecular weight, which led to the pre-complexation reactions between BDOM and Cr(VI) in biochars and accelerated the adsorption of Cr(VI) on biochar. In addition, HC-BDOM could serve as the electron donor for Cr(VI) reduction and increase the reduction efficiency of Cr(VI) by Fe(II), while PC- and HPC-BDOM preferred to act as the electron acceptor, competing with Cr(VI) for Fe(II) oxidation and decreasing Cr(VI) reduction capacity. Hence, BDOM (especially for HC-BDOM) could play significant roles in Cr-contaminated wastewater and land remediation, such as increasing soil organic matter, stabilizing heavy metals and detoxifying by oxidation-reduction after biochar's application.

Data availability

The data supporting this study are available in the article and ESI.†

Author contributions

The manuscript was written through contributions of all authors. Hui Liu and Ying Wang contributed equally to the writing of the article. All authors have given approval to the final version of the manuscript.

Conflicts of interest

The authors declare no conflicts of interest.

Acknowledgements

The authors acknowledge financial support from the National Natural Science Foundation of China (Project No. 22206002; Project No. 51608002), the Natural Science Foundation of Anhui Province (Project No. 2208085QB64).

References

1 H. Gui, Q. Yang, X. Lu, H. Wang, Q. Gu and J. D. Martín, Spatial distribution, contamination characteristics and ecological-health risk assessment of toxic heavy metals in soils near a smelting area, *Environ. Res.*, 2023, **222**, 115328, DOI: 10.1016/j.envres.2023.115328.

2 J. Zhang, Z. Liu, B. Tian, J. Li, J. Luo, X. Wang, S. Ai and X. Wang, Assessment of soil heavy metal pollution in provinces of China based on different soil types: from normalization to soil quality criteria and ecological risk assessment, *J. Hazard. Mater.*, 2023, **441**, 129891, DOI: 10.1016/j.jhazmat.2022.129891.

3 B. Pushkar, P. Sevak, S. Parab and N. Nilkanth, Chromium pollution and its bioremediation mechanisms in bacteria: a review, *J. Environ. Manage.*, 2021, **287**, 112279, DOI: 10.1016/j.jenvman.2021.112279.

4 G. Kanagaraj and L. Elango, Chromium and fluoride contamination in groundwater around leather tanning industries in southern India: implications from stable isotopic ratio δ53Cr/δ52Cr, geochemical and geostatistical modelling, *Chemosphere*, 2019, **220**, 943–953, DOI: 10.1016/j.chemosphere.2018.12.105.

5 A. Ramirez, R. Ocampo, S. Giraldo, E. Padilla, E. Flórez and N. Acelas, Removal of Cr(VI) from an aqueous solution using an activated carbon obtained from teakwood sawdust: kinetics, equilibrium, and density functional theory calculations, *J. Environ. Chem. Eng.*, 2020, **8**, 103702, DOI: 10.1016/j.jece.2020.103702.

6 R. N. Bharagava and S. Mishra, Hexavalent chromium reduction potential of *Cellulosimicrobium* sp. isolated from common effluent treatment plant of tannery industries, *Ecotoxicol. Environ. Saf.*, 2018, **147**, 102–109, DOI: 10.1016/j.ecoenv.2017.08.040.

7 X. Guan, H. Dong and J. Ma, Influence of phosphate, humic acid and silicate on the transformation of chromate by Fe(II) under suboxic conditions, *Sep. Purif. Technol.*, 2011, **78**, 253–260, DOI: 10.1016/j.seppur.2011.02.031.

8 W. Liu, J. Li, J. Zheng, Y. Song, Z. Shi, Z. Lin and L. Chai, Different pathways for Cr(III) oxidation: implications for Cr(VI) reoccurrence in reduced chromite ore processing residue, *Environ. Sci. Technol.*, 2020, **54**, 11971–11979, DOI: 10.1021/acs.est.0c01855.

9 H. M. Conesa and I. Párraga-Aguado, Effects on metal availability of the application of tree biochar and municipal waste biosolid in a metalliferous mine tailings substrate, *Environ. Geochem. Health*, 2022, **44**, 1317–1327, DOI: 10.1007/s10653-021-00967-2.

10 A. Peñalver-Alcalá, J. Á. Álvarez-Rogel, H. M. Conesa and M. N. González-Alcaraz, Biochar and urban solid refuse ameliorate the inhospitality of acidic mine tailings and foster effective spontaneous plant colonization under semiarid climate, *J. Environ. Manage.*, 2021, **292**, 112824, DOI: 10.1016/j.jenvman.2021.112824.

11 Z. Phiri, N. T. Moja, T. T. I. Nkambule and L. A. Kock, Utilization of biochar for remediation of heavy metals in aqueous environments: a review and bibliometric analysis, *Heliyon*, 2024, **10**, 25785, DOI: 10.1016/j.heliyon.2024.e25785.

12 T. Bandara, A. Franks, J. Xu, N. Bolan, H. Wang and C. Tang, Chemical and biological immobilization mechanisms of potentially toxic elements in biochar-amended soils, *Crit. Rev. Environ. Sci. Technol.*, 2020, **50**, 903–978, DOI: 10.1080/10643389.2019.1642832.

13 P. He, Q. Yu, H. Zhang, L. Shao and F. Lü, Removal of copper(II) by biochar mediated by dissolved organic matter, *Sci. Rep.*, 2017, **7**, 7091, DOI: 10.1038/s41598-017-07507-y.

14 S. J. Pochampally, E. Letourneau, I. Abdulraheem, J. Monk, D. Sims, S. E. H. Murph, E. J. Marti and J. Moon, Metal–organic-framework and walnut shell biochar composites for lead and hexavalent chromium removal from aqueous environments, *Chemosphere*, 2024, **347**, 143572.

15 N. Chen, S. Cao, L. Zhang, X. Peng, X. Wang, Z. Ai and L. Zhang, Structural dependent Cr(VI) adsorption and reduction of biochar: hydrochar *versus* pyrochar, *Sci. Total Environ.*, 2021, **783**, 147084, DOI: **10.1016/j.scitotenv.2021.147084**.

16 Y. Liu, S. Wu, T. Nguyen, T. Chan, Y. Lu and L. Huang, Biochar mediated uranium immobilization in magnetite rich Cu tailings subject to organic matter amendment and native plant colonization, *J. Hazard. Mater.*, 2022, **427**, 127860, DOI: **10.1016/j.jhazmat.2021.127860**.

17 J. Hou, A. Pugazhendhi, T. N. Phuong, N. C. Thanh, K. Brindhadevi, G. Velu, N. T. L. Chi and D. Yuan, Plant resistance to disease: using biochar to inhibit harmful microbes and absorb nutrients, *Environ. Res.*, 2022, **214**, 113883, DOI: **10.1016/j.envres.2022.113883**.

18 B. Zheng, X. Wang, X. Luo, Z. Wang and B. Xing, Biochar-induced negative carbon mineralization priming effects in a coastal wetland soil: roles of soil aggregation and microbial modulation, *Sci. Total Environ.*, 2018, **610–611**, 951–960, DOI: **10.1016/j.scitotenv.2017.08.166**.

19 Z. Yu, L. Ling, B. P. Singh, Y. Luo and J. Xu, Gain in carbon: deciphering the abiotic and biotic mechanisms of biochar-induced negative priming effects in contrasting soils, *Sci. Total Environ.*, 2020, **746**, 141057, DOI: **10.1016/j.scitotenv.2020.141057**.

20 W. Anupong, K. Jutamas, R. On-uma, M. Alshiekheid, A. Sabour, R. Krishnan, N. T. Chi, A. Pugazhendhi and K. Brindhadevi, Bioremediation competence of *Aspergillus flavus* DDN on pond water contaminated by mining activities, *Chemosphere*, 2022, **304**, 135250, DOI: **10.1016/j.chemosphere.2022.135250**.

21 Q. Yin, M. Liu, Y. Li, H. Li and Z. Wen, Computational study of phosphate adsorption on Mg/Ca modified biochar structure in aqueous solution, *Chemosphere*, 2021, **269**, 129374, DOI: **10.1016/j.chemosphere.2020.129374**.

22 Y. N. Dias, W. V. Pereira, M. V. Costa, E. S. Souza, S. J. Ramos, C. B. Amarante, W. E. O. Campos and A. R. Fernandes, Biochar mitigates bioavailability and environmental risks of arsenic in gold mining tailings from the eastern Amazon, *J. Environ. Manage.*, 2022, **311**, 114840, DOI: **10.1016/j.jenvman.2022**.

23 S. Mia, F. A. Dijkstra and B. Singh, Chapter one–Long-term aging of biochar: a molecular understanding with agricultural and environmental implications, *Adv. Agron.*, 2017, **141**, 1–51, DOI: **10.1016/bs.agron.2016.10.001**.

24 G. Murtaza, Z. Ahmed, M. Usman, Y. Li, A. Tariq and M. Rizwan, Effects of Biotic and Abiotic Aging Techniques on Physiochemical and Molecular Characteristics of Biochar and Their Impacts on Environment and Agriculture: A Review, *J. Soil Sci. Plant Nutr.*, 2023, **23**, 1535–1564, DOI: **10.1007/s42729-023-01201-x**.

25 Y. Yang, K. Sun, L. Han, Y. Chen, J. Liu and B. Xing, Biochar stability and impact on soil organic carbon mineralization depend on biochar processing, aging and soil clay content, *Soil Biol. Biochem.*, 2022, **169**, 108657, DOI: **10.1016/j.soilbio.2022.108657**.

26 B. Choudhary, D. Paul, A. Singh and T. Gupta, Removal of hexavalent chromium upon interaction with biochar under acidic conditions: mechanistic insights and application, *Environ. Sci. Pollut. Res.*, 2017, **24**, 16786–16797, DOI: **10.1007/s11356-017-9322-9**.

27 M. Hori, K. Shozugawa and M. Matsuo, Reduction process of Cr(VI) by Fe(II) and humic acid analyzed using high time resolution XAFS analysis, *J. Hazard. Mater.*, 2015, **285**, 140–147, DOI: **10.1016/j.jhazmat.2014.11.047**.

28 X. Dong, L. Q. Ma, J. Gress, W. Harris and Y. Li, Enhanced Cr(VI) reduction and As(III) oxidation in ice phase: important role of dissolved organic matter from biochar, *J. Hazard. Mater.*, 2014, **267**, 62–70, DOI: **10.1016/j.jhazmat.2013.12.027**.

29 Q. Wang, Y. Li, Z. Yu, X. Li, S. Yin, W. Ji, Y. Hu, W. Cai and X. Wang, Highly porous carbon derived from hydrothermal–pyrolysis synergistic carbonization of biomass for enhanced CO_2 capture, *Colloids Surf., A*, 2023, **673**, 131787, DOI: **10.1016/j.colsurfa.2023.131787**.

30 K. Serelis, N. Mantzos, D. Meintani and I. Konstantinou, The effect of biochar, hydrochar particles and dissolved organic matter on the photodegradation of metribuzin herbicide in aquatic media, *J. Environ. Chem. Eng.*, 2021, **9**, 105027, DOI: **10.1016/j.jece.2021.105027**.

31 X. Gui, C. Liu, F. Li and J. Wang, Effect of pyrolysis temperature on the composition of DOM in manure-derived biochar, *Ecotoxicol. Environ. Saf.*, 2020, **197**, 110597, DOI: **10.1016/j.ecoenv.2020.110597**.

32 K. Sun, M. Kang, Z. Zhang, J. Jin, Z. Wang, Z. Pan, D. Xu, F. Wu and B. Xing, Impact of deashing treatment on biochar structural properties and potential sorption mechanisms of phenanthrene, *Environ. Sci. Technol.*, 2013, **47**, 11473–11481, DOI: **10.1021/es4026744**.

33 S. Wang, L. Jiao, S. Yang, X. Jin, H. Liang and F. Wu, Organic matter compositions and DOM release from the sediments of the shallow lakes in the middle and lower reaches of Yangtze River region, China, *Appl. Geochem.*, 2011, **26**, 1458–1463, DOI: **10.1016/j.apgeochem.2011.05.019**.

34 A. A. Khan, S. R. Naqvi, I. Ali, M. Arshad, H. AlMohamadi and U. Sikandar, Algal-derived biochar as an efficient adsorbent for removal of Cr(VI) in textile industry wastewater: non-linear isotherm, kinetics and ANN studies, *Chemosphere*, 2023, **316**, 137826, DOI: **10.1016/j.chemosphere.2023.137826**.

35 C. He, X. He, J. Li, Y. Luo, J. Li, Y. Pei and J. Jiang, The spectral characteristics of biochar-derived dissolved organic matter at different pyrolysis temperatures, *J. Environ. Chem. Eng.*, 2021, **9**, 106075, DOI: **10.1016/j.jece.2021.106075**.

36 D. Wan, J. Wang, D. D. Dionysios, Y. Kong, W. Yao, S. Selvinsimpson and Y. Chen, Photogeneration of reactive species from biochar-derived dissolved black carbon for

the degradation of amine and phenolic pollutants, *Environ. Sci. Technol.*, 2021, **55**, 8866–8876, DOI: 10.1021/acs.est.1c01942.

37 H. Zhang, W. Qian, L. Wu, S. Yu, R. Wei, W. Chen and J. Ni, Spectral characteristics of dissolved organic carbon (DOC) derived from biomass pyrolysis: Biochar-derived DOC *versus* smoke-derived DOC, and their differences from natural DOC, *Chemosphere*, 2022, **302**, 134869, DOI: 10.1016/j.chemosphere.2022.134869.

38 M. Huang, Z. Li, N. Luo, R. Yang, J. Wen, B. Huang and G. Zeng, Application potential of biochar in environment: insight from degradation of biochar-derived DOM and complexation of DOM with heavy metals, *Sci. Total Environ.*, 2019, **646**, 220–228, DOI: 10.1016/j.scitotenv.2018.07.282.

39 Y. Wang, Y. Hu, C. Yang, Q. Wang and D. Jiang, Variations of DOM quantity and compositions along WWTPs-river-lake continuum: implications for watershed environmental management, *Chemosphere*, 2019, **218**, 468–476, DOI: 10.1016/j.chemosphere.2018.11.037.

40 J. Gao, Z. Wang, B. Li, W. Zhao, Z. Ba, Z. Liu, J. Huang and Y. Fang, Effect of hydrothermal pH values on the morphology of special microspheres of lignin-based porous carbon and the mechanism of carbon dioxide adsorption, *Bioresour. Technol.*, 2024, **393**, 130171, DOI: 10.1016/j.biortech.2023.130171.

41 A. Shakya, M. Vithanage and T. Agarwal, Influence of pyrolysis temperature on biochar properties and Cr(VI) adsorption from water with groundnut shell biochars: mechanistic approach, *Environ. Res.*, 2022, **215**, 114243, DOI: 10.1016/j.envres.2022.114243.

42 M. Fan, C. Li, Y. Sun, L. Zhang and S. Zhang, *In situ* characterization of functional groups of biochar in pyrolysis of cellulose, *Sci. Total Environ.*, 2021, **799**, 149354, DOI: 10.1016/j.scitotenv.2021.149354.

43 X. Yang, Z. Guo, X. Chen, S. Xi, K. Cui, J. Li, D. Dong, F. Wu and Z. Wu, Efficient degradation of thiamethoxam pesticide in water by iron and manganese oxide composite biochar activated persulfate, *Chem. Eng. J.*, 2023, **473**, 145051, DOI: 10.1016/j.cej.2023.145051.

44 H. Hyewon, J. Lee, M. A. Ahmed and J. W. Choi, Evaluation of pyrochar and hydrochar derived activated carbons for biosorbent and supercapacitor materials, *J. Environ. Manage.*, 2021, **298**, 113436, DOI: 10.1016/j.jenvman.2021.113436.

45 R. M. Duarte, E. B. Santos and A. C. Duarte, Spectroscopic characteristics of ultrafiltration fractions of fulvic and humic acids isolated from an eucalyptus bleached Kraft pulp mill effluent, *Water Res.*, 2003, **37**, 4073–4080, DOI: 10.1016/S0043-1354(03)00411-1.

46 K. Wang, W. Li, X. Gong, Y. Li, C. Wu and N. Ren, Spectral study of dissolved organic matter in biosolid during the composting process using inorganic bulking agent: UV-Vis, GPC, FTIR and EEM, *Int. Biodeterior. Biodegrad.*, 2013, **85**, 617–623, DOI: 10.1016/j.ibiod.2013.03.033.

47 C. Song, S. Shan, C. Yang, C. Zhang, X. Zhou, Q. Ma, K. Yrjälä, H. Zheng and Y. Cao, The comparison of dissolved organic matter in hydrochars and biochars from pig manure, *Sci. Total Environ.*, 2020, **720**, 137423, DOI: 10.1016/j.scitotenv.2020.137423.

48 Y. Liu, S. Ma and J. Chen, A novel pyro-hydrochar *via* sequential carbonization of biomass waste: preparation, characterization and adsorption capacity, *J. Cleaner Prod.*, 2018, **176**, 187–195, DOI: 10.1016/j.jclepro.2017.12.090.

49 F. Yang, C. Wang and H. Sun, A comprehensive review of biochar-derived dissolved matters in biochar application: production, characteristics, and potential environmental effects and mechanisms, *J. Environ. Chem. Eng.*, 2021, **9**, 105258, DOI: 10.1016/j.jece.2021.105258.

50 G. Tan and H. Yu, Rethinking biochar: black gold or not?, *Nat. Rev. Mater.*, 2023, **9**, 4–5, DOI: 10.1038/s41578-023-00634-1.

51 P. Viotti, S. Marzeddu, A. Antonucci, M. A. Décima, P. Lovascio, F. Tatti and M. R. Boni, Biochar as alternative material for heavy metal adsorption from groundwaters: lab-scale (column) experiment review, *Materials*, 2024, **17**, 809, DOI: 10.3390/ma17040809.

52 K. H. Hama Aziz and R. Kareem, Recent advances in water remediation from toxic heavy metals using biochar as a green and efficient adsorbent: a review, *Case Stud. Chem. Environ. Eng.*, 2023, **8**, 100495, DOI: 10.1016/j.cscee.2023.100495.

53 P. Liao, W. Li, Y. Jiang, J. Wu, S. Yuan, J. D. Fortner and D. E. Giammar, Formation, aggregation, and deposition dynamics of nom-iron colloids at anoxic-oxic interfaces, *Environ. Sci. Technol.*, 2017, **51**, 12235–12245, DOI: 10.1021/acs.est.7b02356.

54 Y. Chen, K. Sun, Y. Yang, B. Gao and H. Zheng, Effects of biochar on the accumulation of necromass-derived carbon, the physical protection and microbial mineralization of soil organic carbon, *Crit. Rev. Environ. Sci. Technol.*, 2024, **54**, 39–67, DOI: 10.1080/10643389.2023.2221155.

55 A. El-Naggar, A. H. El-Naggar, S. M. Shaheen, B. Sarkar, S. X. Chang, D. C. W. Tsang, J. Rinklebe and Y. S. Ok, Biochar composition-dependent impacts on soil nutrient release, carbon mineralization, and potential environmental risk: a review, *J. Environ. Manage.*, 2019, **241**, 458–467, DOI: 10.1016/j.jenvman.2019.02.044.

56 Y. Sun, X. Xiong, M. He, Z. Xu, D. Hou, W. Zhang, Y. S. Ok, J. Rinklebe, L. Wang and D. C. Tsang, Roles of biochar-derived dissolved organic matter in soil amendment and environmental remediation: a critical review, *Chem. Eng. J.*, 2021, **424**, 130387, DOI: 10.1016/j.cej.2021.130387.

57 T. E. Sackett, N. Basiliko, G. L. Noyce, C. Winsborough, J. Schurman, C. Ikeda and S. C. Thomas, Soil and greenhouse gas responses to biochar additions in a temperate hardwood forest, *GCB Bioenergy*, 2015, **7**, 1062–1074, DOI: 10.1111/gcbb.12211.

58 L. Ling, Y. Luo, B. Jiang, J. Lv, C. Meng, Y. Liao, B. J. Reid, F. Ding, Z. Lu, Y. Kuzyakov and J. Xu, Biochar induces mineralization of soil recalcitrant components by activation of biochar responsive bacteria groups, *Soil Biol. Biochem.*, 2022, **172**, 108778, DOI: 10.1016/j.soilbio.2022.108778.

59 M. B. Soares, C. E. P. Cerri, J. A. M. Dematte and L. R. F. Alleoni, Biochar aging: impact of pyrolysis temperature on sediment carbon pools and the availability of arsenic and lead, *Sci. Total Environ.*, 2022, **807**, 151001, DOI: **10.1016/j.scitotenv.2021.151001**.

60 X. Zheng, J. Dong, W. Zhang, J. Xiang, X. Yin and L. Han, Biogas residue biochar shifted bacterial community, mineralization, and molecular structure of organic carbon in a sandy loam Alfisol, *GCB Bioenergy*, 2021, **13**, 838–848, DOI: **10.1111/gcbb.12813**.

61 X. Huang, B. Xu, S. Zhu, F. Ma and C. Jin, Overlooked contributions of biochar-derived dissolved organic matter on the adsorption of Pb(II): impacts of fractionation and interfacial force, *J. Hazard. Mater.*, 2021, **420**, 126692, DOI: **10.1016/j.jhazmat.2021.126692**.

62 J. Fang, L. Cheng, R. Hameed, L. Jin, D. Wang, G. Owens and D. Lin, Release and stability of water dispersible biochar colloids in aquatic environments: effects of pyrolysis temperature, particle size, and solution chemistry, *Environ. Pollut.*, 2020, **260**, 114037, DOI: **10.1016/j.envpol.2020.114037**.

63 N. Liu, Y. Zhang, C. Xu, P. Liu, J. Lv, Y. Liu and Q. Wang, Removal mechanisms of aqueous Cr(VI) using apple wood biochar: a spectroscopic study, *J. Hazard. Mater.*, 2020, **384**, 121371, DOI: **10.1016/j.jhazmat.2019.121371**.

64 Y. Zhang, X. Xu, L. Cao, Y. S. Ok and X. Cao, Characterization and quantification of electron donating capacity and its structure dependence in biochar derived from three waste biomasses, *Chemosphere*, 2018, **211**, 1073–1081, DOI: **10.1016/j.chemosphere.2018.08.033**.